International Journal of Concrete Structures and Materials

RESEARCH Open Access

Performance of Rubberized RC Beams Flexural-Strengthened Using Near-Surface Mounted Systems

Mohamed Emara[1*], Abdulrahman H. Mostafa[1], Heba A. Mohamed[1] and Mahmoud Zaghlal[1]

Abstract

This research investigates the flexural performance of strengthened rubberized concrete beams via bottom, side, and hybrid near-surface mounted (NSM) approaches using GFRP/steel rebars. Eleven strengthened specimens, alongside one control, were subjected to four-point loading setup till failure. The investigation focused on three key parameters: strengthening technique (bottom, side, or hybrid), NSM bar area, and bar type (GFRP or steel). The results revealed significant improvements across various performance metrics. It was demonstrated that NSM strengthening enhanced the beam's cracking loads by up to 90%. Correspondingly, the strengthened beam's yield and ultimate loads witnessed enhancements up to 48% and 79%, respectively. Notably, the load-carrying ability of GFRP bars consistently outperformed steel bars. Additionally, increasing the quantity of NSM strengthening proved beneficial, with bottom placement offering a slight advantage due to a larger internal lever arm. The proposed hybrid NSM technique, employing three 8-mm-diameter GFRP bars, emerged as the most effective strengthening scheme. However, utilizing four bars resulted in decreased effectiveness due to overlapping tensile stresses and accelerated debonding failure. Finally, the experimental results were compared to analytical predictions, with close agreement observed. The experimental-to-predicted analytical result ratio varies from 0.84 to 1.01%, indicating the validity of the analytical approach.

Keywords Strengthening, NSM, SNSM, Flexural behavior, GFRP bars, Rubberized concrete, Hybrid

1 Introduction

Structural strengthening is the process of improving a structure's resistance to current or future loads. Strengthening may be needed for different reasons, including deterioration, change of functionality, and errors during the construction procedure (Almusallam et al., 2013; Kusuma et al., 2022).

Previous studies have shown that using fiber reinforcement polymers (FRPs) for strengthening reinforced concrete (RC) elements proved effective. FRPs have been commonly relied on to strengthen RC elements because of the excellent strength-to-weight ratio, simple installation, and high resistance to corrosion (Attari et al., 2012; Reda et al., 2016; Siddika et al., 2020). The most common FRP strengthening methods for improving the flexure strength of RC elements are externally bonded reinforcement (EBR) and near-surface mounted (NSM) techniques. Both approaches involve bonding the strengthening element to the tensile face.

Several studies have examined the efficacy of applying EB FRP laminates or sheets to strengthen RC elements (Abdalla et al., 2020, 2023; Assad et al., 2024; Ceroni & Pecce, 2012; Domenico et al., 2014; Emara et al., 2021, 2022, 2023a, 2023b; Hawileh et al., 2014, 2015, 2018, 2024; Kotynia, 2012; Mhanna et al., 2019; Mostofinejad

Journal information: ISSN 1976-0485 / eISSN 2234-1315.

*Correspondence:
Mohamed Emara
mremara@eng.zu.edu.eg
[1] Structural Engineering Department, Faculty of Engineering, Zagazig University, Zagazig 44519, Egypt

& Moghaddas, 2014; Nawaz et al., 2022; Nayak et al., 2018; Saqan et al., 2013). One major drawback of the EBR method is its tendency to experience premature debonding, which limits the FRP strengthening maximum capacity. Furthermore, this method has its downsides, including the pretreatment procedures, installation time, the alteration of the structural members' appearance, and vulnerability to thermal, climatic, and mechanical damage.

The bottom NSM (BNSM) method is implemented by trimming grooves in the bottom concrete layer and installing FRP bars or strips with proper filler, usually epoxy adhesive or mortar (Lorenzis, 2000). According to several studies (Darain et al., 2015; Hosen et al., 2015a, 2015b, 2016a, 2016b, 2023a; Rahman et al., 2016), in comparison to the EBR, the BNSM-FRP system is considered an effective alternative as it requires less surface preparation, enhances protection against external damage, and, while premature debonding failure is not avoided, the bond capacity is improved, thereby increasing the FRP utilization (Al-Saadi et al., 2019; Barros et al., 2007; Bilotta et al., 2011, 2015; Gopinath et al., 2016; Lorenzis & Teng, 2007; Zhang et al., 2017).

Khalifa (2016) evaluated the efficacy of BNSM and EBR techniques using carbon FRP (CFRP) to improve the flexural characteristics of RC beams. While the BNSM-CFRP strengthened beams exhibited increased ultimate loads, their failure mode involved debonding and concrete cover peeling, highlighting limitations in this approach.

In their study, Tang et al. (2006) analyzed how the bending performance of the BNSM-strengthened beams was affected by the concrete type, reinforcing rebars (GFRP and steel), and adhesive. Their findings revealed significant improvements in ultimate capacity, ranging between 23 and 53% compared to control beams.

In their investigation of RC beam flexural behavior using BNSM technique, Sharaky et al. (2015) employed both GFRP and CFRP bars. They tested beams with both partially bonded and fully bonded BNSM bars to understand the influence of bond behavior on flexural performance. The stiffness and bearing capacity of fully bonded reinforcements were higher. It was noted that the reinforced samples experienced failure due to concrete cover separation, concrete splitting, and debonding occurring at the epoxy–concrete interface.

Although studies have shown that the BNSM system could considerably enhance the bending behavior of RC beams, this system may have some limitations. According to ACI 440.2R (2017), NSM systems require grooves no less than 1.5 times the bar diameter, clear groove spacing more than twice the groove depth to evade tensile stress overlap, and clear edge distance four times the groove depth to diminish edge effects, which implies the need for adequate width of the RC beams, which may not be available in practice. Furthermore, the BNSM system may not be feasible, particularly when the beam widths are occupied by partitions such as brick walls.

Hosen et al., (2015c, 2017a, 2018, 2019, 2020, 2023b) and Shukri et al., (2016) employed the side near surface mounted (SNSM) approach as an alternative way to overcome the limitations of the BNSM system. Counter to the BNSM system, this approach involves inserting the reinforcement into grooves provided to the beam sides rather than bottom. The results of the experiments revealed that the SNSM approach notably improved the behavior and ensured ductile failure. Comparing the steel bars to the CFRP bars, the former showed greater ductility.

According to Sabau et al. (2018), their investigation into SNSM and BNSM techniques revealed that SNSM efficiently addressed the issue of concrete cover separation in tested beams. This not only improved the overall capacity of the beams, but also enhanced their energy dissipation capabilities.

Hosen et al. (2017b) demonstrated that the SNSM technique significantly enhances the capacity, energy absorption, toughness, and deformability of structures. Notably, their study revealed that the bonded length among the strengthening reinforcement and the original element contributes more significantly to improve flexural behavior compared to the amount of reinforcement used.

Partially replacing natural aggregates in concrete with crumb rubber from recycled tires is one of the acceptable solutions for its safe disposal to protect the environment and preserve the aggregates. Although there are concerns about the reduction of concrete's strength in compression and tension, as well as its elastic modulus, integrating rubber tires, partially replacing both coarse and fine aggregates, offers promising improvements for concrete structures. These benefits include enhanced deformability, increased energy absorption, and improved impact resistance. Additionally, the resulting mix boasts a lower unit weight and suitable workability compared to conventional concrete (Gerges et al., 2018; Mendis et al., 2017a; Toutanji, 1996; Xue & Shinozuka, 2013). Limiting rubber content to a maximum of 20% by volume of fine aggregates is recommended to minimize its influence on the concrete mechanical characteristics (Khatib & Bayomy, 1999; Mustafa et al., 2020).

Mendis et al. (2017b) investigated reinforced rubberized concrete beams' flexural behavior. Results revealed that the ultimate bending capacity of the beams remained largely unchanged by quantity of rubber utilized. Furthermore, the flexural capacity and cracking load of rubberized concrete could be predicted accurately using the current design guidelines.

Table 1 Mix proportions

Concrete	Cement (kg/m^3)	Fine aggregate (kg/m^3)	Coarse aggregate (kg/m^3)	Water/cement (ratio)	Crumb rubber (kg/m^3)	Super- plasticizer (kg/m^3)
RUC	400	600	1100	0.40	28	2.0

Sharaky et al. (2020) evaluated the effects of the crumb rubber ratio on the performance of RC beams. The study discovered that adding crumb rubber particles as a partial replacement of fine aggregate reduced load capacity. However, utilizing welded wire mesh as shear reinforcement enhanced beam capacity and switched failure from shear to flexural.

This study investigates the flexural performance of RC beams incorporating rubber. The goal is twofold: to leverage the potential environmental benefits of rubber and to mitigate any drawbacks associated with its use in RC structures. The research examines beams strengthened with two different techniques employing NSM systems: a bottom NSM system, a side NSM system, and a hybrid system that combines both approaches. The investigation was carried out by studying key parameters such as (strengthening distribution, strengthening area, and strengthening material). The results are comprehensively analyzed considering several key aspects: load capacities achieved, load–deflection behavior, observed failure modes, ductility index, and energy absorption capacity.

2 Experimental Program

2.1 Materials Characteristics

2.1.1 Mix Proportions

The current investigation utilized a rubberized concrete mix (RUC), with the proportions shown in Table 1 presenting 15% replacement level of fine natural aggregates with slight adjustments to the mix presented in Yasser et al. (2023). The mix constituents include Ordinary Portland Cement (CEM I 42.5), locally available dolomite as coarse aggregate, clean sand as fine aggregate, potable water, crumb rubber, and superplasticizer. The dolomite had a maximum size of 15 mm and a specific gravity of 2.67. The natural sand was clean, with a fineness modulus of 2.5 and a specific gravity of 2.65. The crumb rubber used was manufactured with sizes between 1 and 2 mm, and a relative density of 0.9 as provided by the manufacturer (Marso-Egypt). High range water-reducer marketed under the name Addicrete BVF utilized to enhance the workability of the mix. The concrete cube testing was performed according to BS EN 12390-3 (2009a), with standard 150 mm×150 mm×150 mm cubic specimens. The cube's 28-day average compressive strength was 29.78 MPa. The splitting tensile tests was carried out in accordance with BS EN 12390-6 (2009b), with standard 150 mm diameter×300 mm height cylinders. The cylinder's average tensile splitting strength was 2.46 MPa.

Table 2 Technical data of Kemapoxy 165 at 25 °C

Property	Kemapoxy 165
Density	1.95 ± 0.02 kg/l
Compressive strength (MPa)	> 80
Flexure strength (MPa)	> 40
Adhesive strength on concrete (MPa)	10.3

Table 3 Steel and GFRP reinforcement properties

Bar material	Diameter (mm)	Yield stress (MPa)	Ultimate stress (MPa)	Ultimate strain	Young's modulus (GPa)
Steel	8	280	420	22.00%	200
	12	420	600	15.00%	200
GFRP	6, 8, 10	-	1000	2.13%	47

2.2 Epoxy Adhesive

The strengthening steel/GFRP bars were attached to the concrete using a two-component epoxy resin, commercially named Kemapoxy 165, with a 12:1 mixing ratio. Specifications for the resin are shown in Table 2 based on supplier data sheets.

2.3 Reinforcement

High-grade steel rebars of 12 mm were employed as internal tensile reinforcement. 8 mm mild steel bars were utilized as internal compression reinforcement, transverse stirrups and were utilized in the flexural strengthening of the RC beam specimens. Three GFRP bar sizes 6, 8 and 10 mm were utilized in strengthening the concrete beams. Table 3 summarizes steel and GFRP reinforcement properties reported by the supplier.

2.4 Test Matrix

This study investigated 11 concrete specimens in all. The specimens were classified into five sets according to the strengthening technique and type of strengthening bars. For the first set, one specimen was kept un-strengthened as a control for comparison purposes. The second set contains three specimens strengthened with two

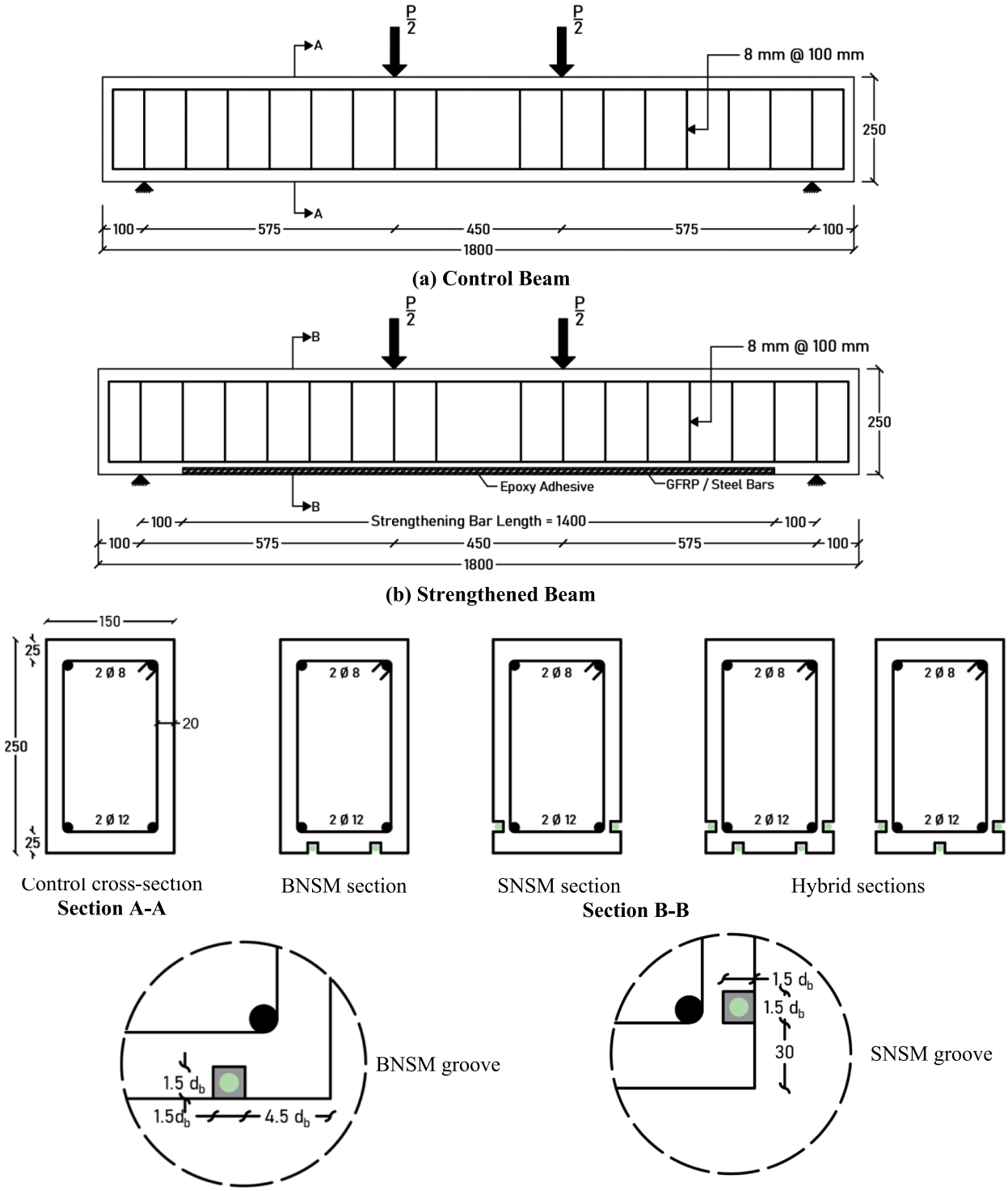

Fig. 1 Test specimens detailing

GFRP bars through the BNSM approach to investigate the influence of GFRP bar diameter (6, 8, and 10 mm). The third set was designed similarly to the second one except that the strengthening was applied through the SNSM technique as shown in Fig. 1. For the fourth set, two beams were strengthened using BNSM and SNSM techniques, respectively, by applying two steel bars of size 8 mm. For the fifth set, two beams were strengthened

with hybrid NSM technique: the first with three 8 mm GFRP bars and the second with four 8 mm GFRP bars, as illustrated in Fig. 1. Table 4 presents the experimental test matrix for the experimented specimens.

2.5 Beams Configuration

Figure 1 depicts the size and reinforcing scheme of experimented beams. Beams measured 150 mm × 250 mm in cross-section, had a total length of 1800 mm, a clear span of 1600 mm, and a shear span of 575 mm. The beam's internal reinforcement comprises two tension deformed steel bars of 12 mm and two compression mild steel bars of 8 mm. Stirrups of 8 mm were placed every 100 mm throughout the shear span, as shown in Fig. 1**.**

According to ACI 440.2R (2017), the minimum groove dimensions for both BNSM and SNSM-strengthened beams were 1.5 times the size of an NSM bar. For BNSM-strengthened beams, the clear edge distance was retained at 4.5 times the size of the NSM bar to guarantee that the distance between grooves in all BNSM beams is at least twice the groove depth as per ACI 440.2R (Committee, 2017). For SNSM strengthened specimens, the grooves were cut 30 mm above the tension face.

2.6 Strengthening Procedure

The installation of strengthening bars is shown in Fig. 2. The strengthening bars were inserted in longitudinal grooves which were formed during the casting process using square wood strips with the requisite groove dimensions as presented in Fig. 2a. The wooden strips were inserted inside the beam molds prior to casting and then removed after demolding. After 28 days of curing, the test specimens were strengthened with bars. As shown in Fig. 2b**,** prior to inserting the strengthening bars, the grooves were cleaned using a high-pressure air jet. Figure 2c shows how the grooves were partially filled with epoxy resin before the bars were inserted into the grooves with slight force. After applying more epoxy to the slits, a spatula was used to level the surface as illustrated in Fig. 2d. To help attain the full strength of the bonding material, the specimens were examined after 2 weeks of applying the epoxy resin. The bond length for all BNSM and SNSM beams was 1400 mm as shown in Fig. 1.

2.7 Test Setup

The specimens were experimented on in a four-point loading setup using a 2500-kN capacity testing machine as illustrated in Fig. 3. The load applied by the hydraulic machine was distributed to the tested beam via a spreader steel beam. A calibrated load cell was utilized to capture the practical load. The mid-span deflection was monitored using a single linear variable differential transformer (LVDT). A data logger was used for recording the load and deflection measurements.

3 Test Results and Discussion

Table 5 summarizes the test findings with respect to the cracking load (Pcr), the yielding load (Py), the ultimate load (P_u), and their associated deflections (Δcr, Δy, Δu). It ought to be mentioned that the slope variations in the load–deflection curves were used to determine both (Pcr) and (Py). The table also includes the energy absorption capacity (Eab), ductility index (DI), and observed modes of failure.

Table 4 Test matrix

Group	Notation	Strengthening technique	Strengthening bars			Test variables
			Number	Diameter (mm)	Material	
Control	CB	Control beam (un-strengthened)				Control beam
G1	BNG2-8	BNSM	2	8	GFRP	BNSM technique
	BNG2-6			6		BNSM technique and strengthening area
	BNG2-10			10		BNSM technique and strengthening area
G2	SNG2-8	SNSM	2	8	GFRP	SNSM technique
	SNG2-6			6		SNSM technique and strengthening area
	SNG2-10			10		SNSM technique and strengthening area
G3	BNS2-8	BNSM	2	8	Steel	BNSM technique and strengthening material
	SNS2-8	SNSM				SNSM Technique and strengthening material
G4	BSNG3-8	Hybrid (BNSM and SNSM)	3	8	GFRP	Hybrid technique and strengthening area
	BSNG3-4		4	8	GFRP	Hybrid technique and strengthening area

(a) Using square wood strips with the requisite groove dimensions

(b) Grooves were cleaned using a high-pressure air jet

(c) Grooves were partially filled with epoxy resin before inserting bars

(d) Using square wood strips with the requisite groove dimensions

Fig. 2 Strengthening procedure in lab

3.1 Load Capacity

As presented in Table 5, strengthening beams utilizing the NSM approach outperformed the control beam in terms of cracking, yielding, and ultimate loading values.

For beams in group G1, strengthened with the BNSM technique, the beam BNG2-8, which had two bottom 8-mm-diameter GFRP bars, demonstrated a 45% increase in ultimate loading capacity. Replacing the 8 mm bars with 6 mm and 10 mm in beams BNG2-6 and BNG2-10, the ultimate capacity increased by 35% and 78%, respectively. This shows that increasing the area of the strengthening reinforcement results in higher ultimate loading values, as expected.

The group G2 beams were strengthened using the SNSM approach. Among these, beam SNG2-8 had a similar reinforcing area as BNG2-8, but the strengthening position was changed from the bottom to the side, showing a 35% improvement in ultimate capacity. The ultimate capacity increased by 18% and 54% when the 8-mm bars were replaced with 6 mm and 10 mm in beams SNG2-6

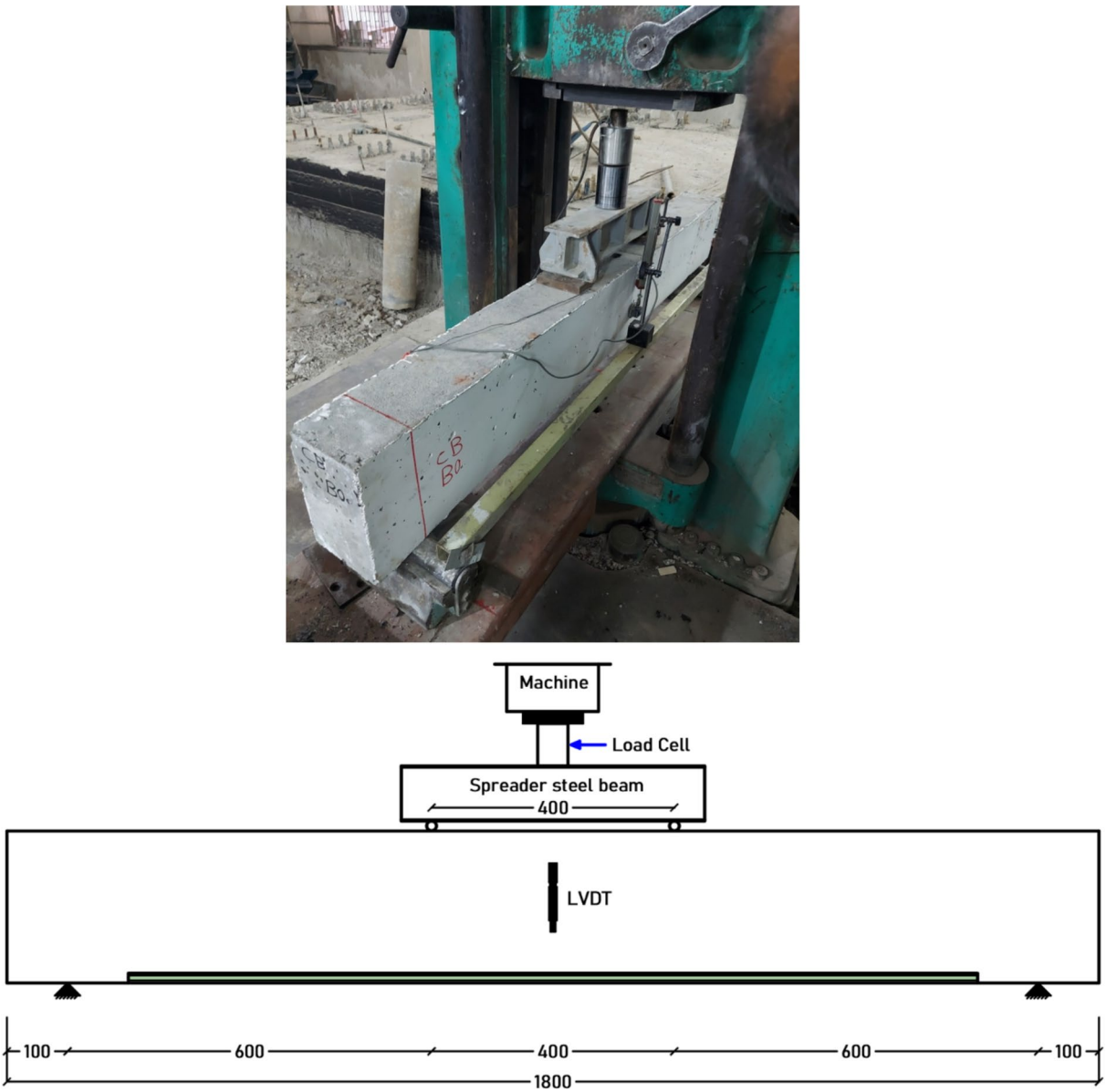

Fig. 3 Test setup

and SNG2-10, respectively. Although the loading capacity increased with increasing the area of the strengthening reinforcement, similar to G1, the enhancement for G2 SNSM-strengthened beams (18–54)% was less than that of G1 BNSM-strengthened beams (35–78%). This was attributed to the lower internal lever arm, which decreased strengthening efficiency.

The beams from group G3 were strengthened with two bottom 8 mm steel bars utilizing both BNSM and SNSM techniques for BNS2-8 and SNS2-8 beams, respectively. These techniques resulted in a 34% and 29% enhancement in ultimate capacity for the BNS2-8 and SNS2-8 beams, respectively, with the BNSM technique proving to be more efficient. In comparison to the beams BNG2-8 and SNG2-8, the GFRP-strengthened beams demonstrated higher capacities due to GFRP's higher ultimate strength than steel.

Group G4 beams were strengthened using a hybrid NSM technique. The beam BSNG3-8 was strengthened using three 8-mm-diameter GFRP bars (one at the bottom and two on the sides), resulting in a 79% increase in ultimate capacity. On the other hand, beam BSNG4-8, although it was strengthened with four 8-mm-diameter GFRP bars (two at the bottom and two on the sides),

Table 5 Experimental results

Group	Notation	Pcr (kN)	Δcr (mm)	Py (kN)	Δy (mm)	Pu (kN)	Δu (mm)	Eab (kN mm)	DI	Failure mode
Control	CB	19.9	0.30	66.1	4.60	78.6	34.00	2398	7.39	CC
G1	BNG2-8	29.1 (1.46)	0.72	85.5 (1.29)	5.98	114.2 (1.45)	22.56	2055	3.77	CS → CC
	BNG2-6	26.8 (1.35)	0.78	75.7 (1.15)	5.00	104.6 (1.35)	20.24	1665	4.05	ED → CC
	BNG2-10	32.1 (1.61)	1.02	86.6 (1.31)	5.70	139.8 (1.78)	20.94	2063	3.67	CS → CC
G2	SNG2-8	28.0 (1.41)	0.64	72.6 (1.10)	4.22	106.3 (1.35)	17.28	1408	4.09	CC → ED
	SNG2-6	23.3 (1.17)	0.68	71.7 (1.08)	4.60	93.0 (1.18)	20.10	1520	4.37	CC → ID
	SNG2-10	29.3 (1.47)	0.54	78.6 (1.19)	4.65	120.8 (1.54)	18.25	1643	3.92	CC → ED
G3	BNS2-8	33.9 (1.70)	0.66	97.6 (1.48)	5.18	105.3 (1.34)	20.64	1902	3.98	CC → CS
	SNS2-8	32.4 (1.63)	0.60	91.8 (1.39)	5.32	101.6 (1.29)	22.34	1990	4.20	CC
G4	BSNG3-8	35.2 (1.77)	1.04	82.1 (1.24)	5.00	140.9 (1.79)	29.78	3240	5.96	CC → ED
	BSNG4-8	37.8 (1.90)	0.72	89.0 (1.35)	4.78	134.6 (1.71)	17.58	1775	3.68	CCS

The values in parentheses represent the ratio of the recorded load of the reinforced specimen to the control load

CC concrete crushing, *CS* concrete splitting, *CCS* concrete cover separation, *ED* external debonding, *ID* intermediate debonding

showed only a 71% increase in ultimate capacity due to the overlapping tensile stresses around the strengthening bars and accelerated debonding failure due to the proximity of bottom and side grooves. It is worth noting that the total NSM area in BSNG3-8 is 150.8 mm^2, exhibiting the highest increase in ultimate capacity showing more efficiency than BNG2-10 and SNG2-10 with a total NSM area of 157.1 mm^2. This indicates that the hybrid NSM technique has significant potential.

3.2 Load–Deflection Response

Figure 4 displays the load versus mid-span deflection responses of the examined specimens. All curves present a tri-linear response divided into three stages: pre-cracking, cracking, and post-cracking. The strengthened beams exhibited linear elastic behavior like the reference beam, with no significant impact on stiffness during the pre-cracking stage; however, compared to the reference beam, the initial cracking load increased significantly. During the cracking stage, from first cracking to steel yielding, the strengthening improved the specimen stiffness as well as the yielding load relative to the reference beam. In the post-cracking stage, after the steel yielding, as the applied loads on the beam increased, the mid-span deflection increased at a faster pace than in prior stages. NSM GFRP/steel bars monitored the cracks and their widths during this stage, with bending stiffness gradually decreasing until failure.

Figure 4a presents load–deflection curves for the BNSM GFRP specimens. In the first stage, the strengthened G1 specimens showed a considerable increase of 35–61% in the first cracking load. In the second stage, stiffness was enhanced along with yielding loads by 15–31%. In the third stage, the strengthened specimens demonstrated greater ultimate capacities. However, the ductility index was lower, and there was a drop in the ultimate mid-span deflections of 20.24–22.56 mm compared to the 34.00 mm of the control beam.

Load–deflection curves for the SNSM GFRP specimens are illustrated in Fig. 4b. Similarly, the SNSM GFRP-strengthened beam's cracking and yielding loads increased by 17–47% and 9–19%, respectively, slightly lower than the corresponding G1 specimens. Although the SNSM specimens demonstrated lower ultimate capacities and ultimate mid-span deflections between 17.28 and 20.10 mm, the ductility index was improved compared to the previous BNSM specimens.

Figure 4c shows load–deflection curves for the steel specimens. The first-stage stiffness and cracking loads were higher relative to their equivalent GFRP specimens. The cracking loads of the BNS2-8 specimen increased by 70%, whereas the SNS2-8 specimen showed a slightly lower increase of 63%. Similarly, the second stage showed an enhancement in the stiffness and yielding loads by 48% for BNS2-8 and 39% for SNS2-8. In the third stage, in contrast to the enhanced capacity for yield and cracking loads, strengthened beams with steel bars demonstrated lower ultimate capacities compared to the GFRP specimens. The different slope behavior was due to the higher elastic modulus of the steel strengthening compared to the GFRP strengthening. The ultimate mid-span deflections recorded were 20.64–22.34 mm and the ductility index for the steel specimens was higher than the GFRP specimens.

Load–deflection curves for the hybrid strengthened specimens are shown in Fig. 4d. The hybrid strengthening scheme resulted in a 77% and 24% improvement in cracking and yielding loads, respectively, for the

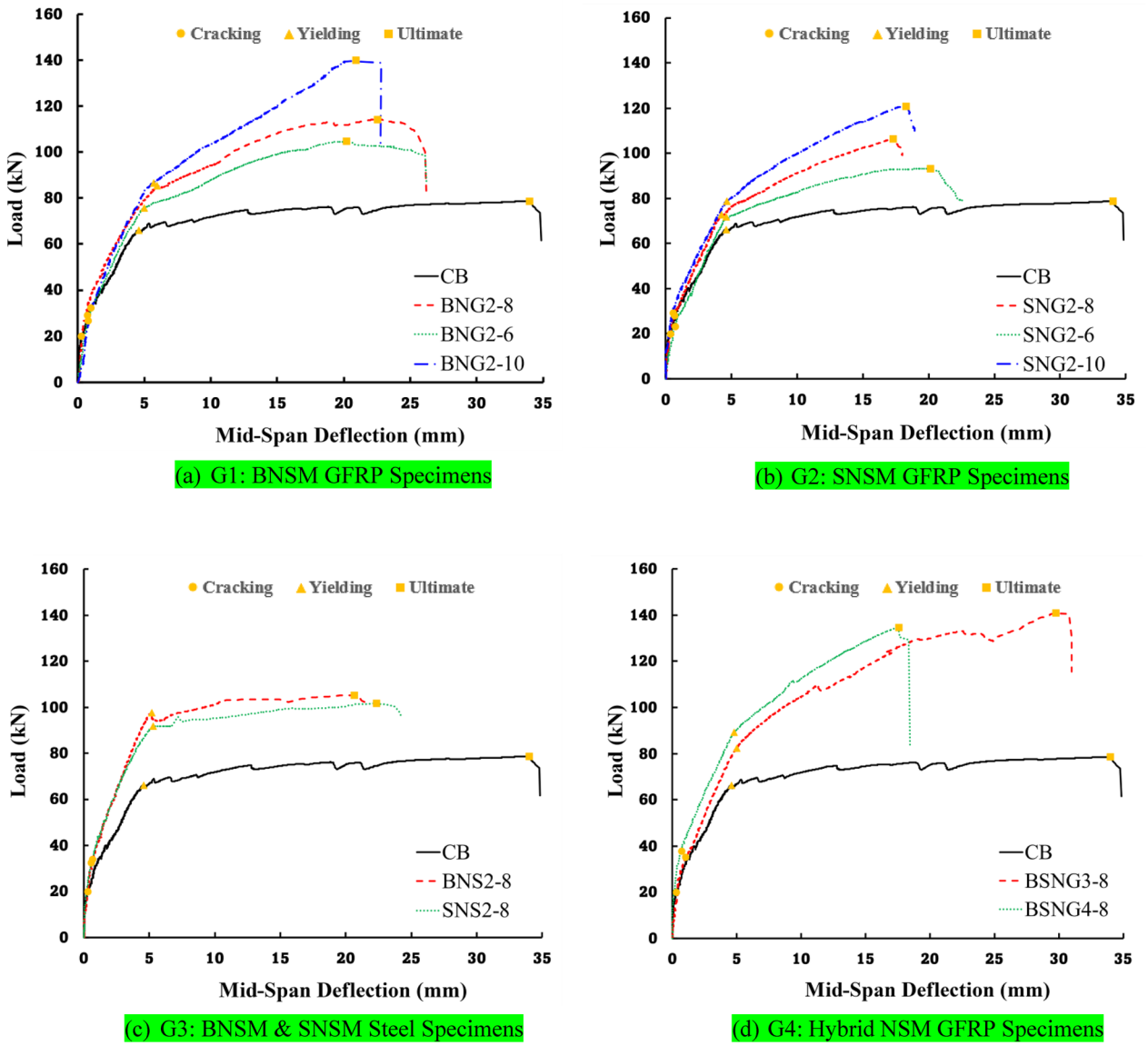

Fig. 4 Load–deflection relationship

BSNG3-8 specimen and a 90% and 35% improvement for the BSNG4-8 specimen, similar to all strengthened beams. BSNG3-8 exhibited the optimum performance exhibiting the highest increase in ultimate capacity with mid-span deflection of 29.78 mm showing the highest ductility index compared to all strengthened specimens. The BSNG4-8 with the highest NSM strengthening area has shown less performance than the BSNG3-8 due to the stress concentrations and premature debonding experiencing an ultimate mid-span deflection of 17.58 mm.

3.3 Modes of Failure

In this study, Fig. 5 illustrates the observed failure mechanisms of all specimens investigated. The reference specimen, as anticipated, experienced the typical flexural failure (yielding of tension steel preceding concrete crushing), as indicated in Fig. 5a. A hairline crack first appeared at midspan, and as the applied stress increased, more cracks emerged. Eventually, failure occurred near the beam's midspan due to the spread of vertical cracks.

For beams in group G1 (BNG2-8, BNG2-6, and BNG2-10), the cracks were thinner in comparison to the reference specimen. However, as the main internal reinforcement yielded, inclined shear cracks developed from the NSM cutoff point,

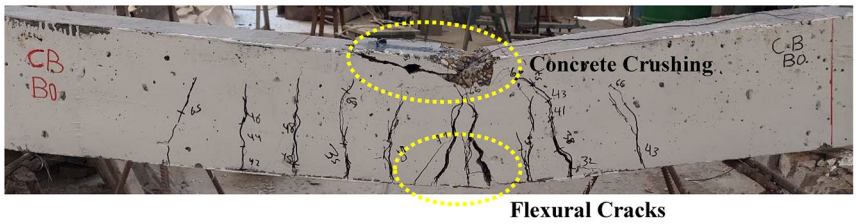

(a) CB

(b) BNG2-8

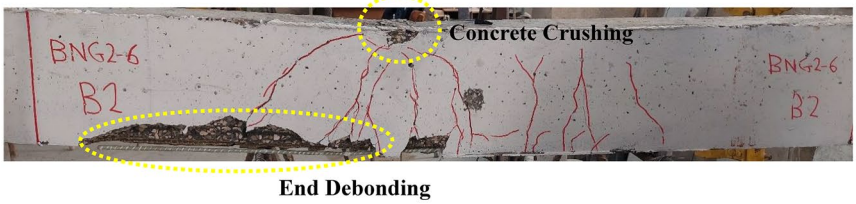

(c) BNG2-6

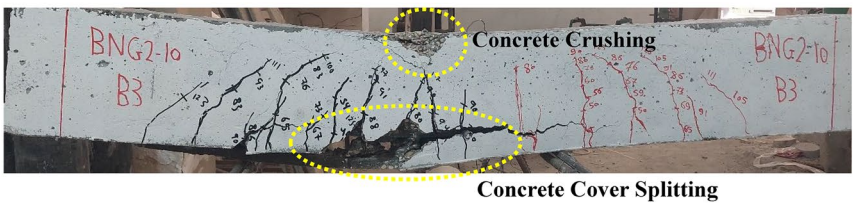

(d) BNG2-10

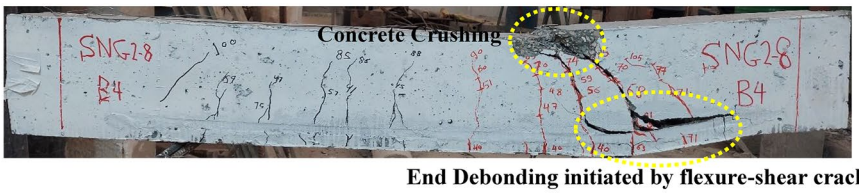

(e) SNG2-8

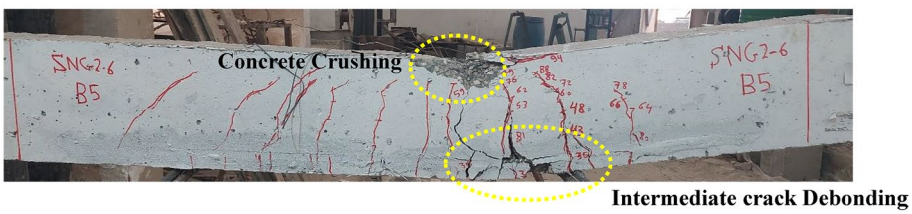

(f) SNG2-6

Fig. 5 Modes of failure of the investigated beams

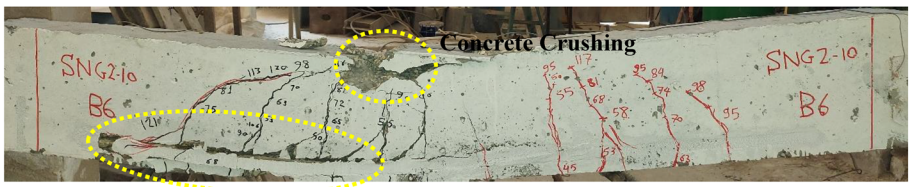

(g) SNG2-10

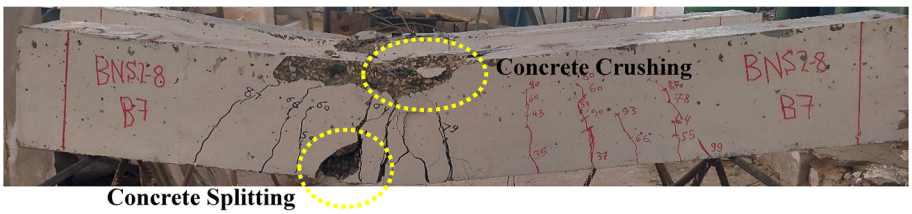

(h) BNS2-8

(i) SNS2-8

(j) BSNG3-8

(k) BSNG4-8

Fig. 5 continued

and the crack's width grew with the applied stress increase. The dominant failure mode for G1 beams was premature debonding followed by crushing of concrete. Specimen BNG2-8 exhibited a concrete cover splitting followed immediately by concrete crushing, as shown in Fig. 5b. As observed in Fig. 5c, the BNSG-6 beam failed by end interfacial debonding followed by concrete crushing. BNG2-10 beam exhibited intermediate concrete cover splitting followed by crushing of concrete above the splitting position, as shown in Fig. 5d.

Adopting the SNSM technique in group G2 (SNG2-8, SNG2-6, and SNG2-10), showed more ductile failure modes compared to G1 specimens, as no evidence of debonding was observed until the compressed concrete had started to crush and the ultimate load was reached. SNG2-8 exhibited concrete crushing at one of the two

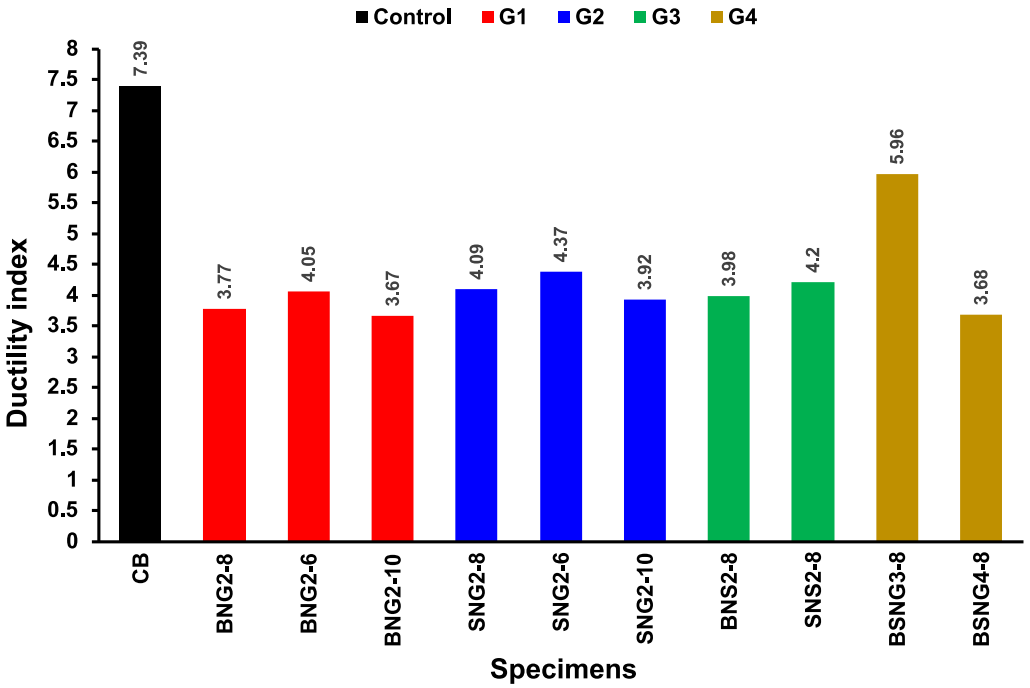

Fig. 6 Ductility index of the investigated beams

load application points, followed by end debonding initiated by the flexure-shear cracks, as illustrated in Fig. 5e. The SNSG-6 beam exhibited an intermediate crack debonding, after failing due to concrete crushing, as shown in Fig. 5f. Similarly, the SNG2-10 beam only exhibited end debonding after the initiation of concrete crushing, as shown in Fig. 5g.

Group G3 beams (BNS2-8 and SNS2-8), followed the same pattern with no debonding observed until reaching the ultimate capacities as G2 specimens. For beam BNS2-8, crushing of the top compressed concrete was initiated adjacent to one of the loading points accompanied by concrete cover splitting just after, as illustrated in Fig. 5h. SNS2-8 beam exhibited concrete crushing between the two loading points with no evidence of any debonding failure, as shown in Fig. 5i.

For group G4 beams, BSNG3-8 showed end debonding failure only after reaching the ultimate capacity and crushing of the compressed top concrete, as shown in Fig. 5j; whereas, for the BSNG4-8 specimen due to the proximity of the side and bottom grooves and the high-stress concentration, a concrete cover separation was exhibited when the shear and normal stresses intersect inducing premature debonding, as shown in Fig. 5k.

3.4 Ductility Index

The ductility index determined from the load–deflection curves shows the ability to withstand inelastic distortions without incurring a significant loss in the capacity to carry loads before failure, offering an indication of approaching collapse (Imjai et al., 2022). The index is computed as the ratio of deflections at ultimate and yielding loads ($\Delta u/\Delta y$) (Sharaky et al., 2020). The results listed in Table 5 enumerate the findings and are depicted graphically in Fig. 6.

All the strengthened beams had a lower ductility index than the reference beam. For G1 specimens (BNG2-8, BNG2-6, and BNG2-10), the decrease in the DI was 49%, 45%, and 50%, respectively. It was noticed that the DI decreased with increasing the strengthening amount. Similarly, for G2 specimens (BNG2-8, BNG2-6, and BNG2-10), the ductility index DI decreased by 45%, 41%, and 47%, respectively. However, the SNSM approach provided more ductile behavior than the BNSM approach, as demonstrated by higher DI values in G2 specimens compared to G1 specimens. It has been observed that replacing GFRP bars with steel bars in G3 specimens has resulted in a higher DI. The decrease in DI for BNS2-8 and SNS2-8 was 46% and 43%, respectively. For G4 specimens, BSNG3-8 has shown the least decrease in DI by only 19% while BSNG4-8 has shown a decrease by 50%.

3.5 Energy Absorption Capacity

Energy absorption capacity is the amount of energy absorbed per unit cross-sectional area of a specimen at extreme

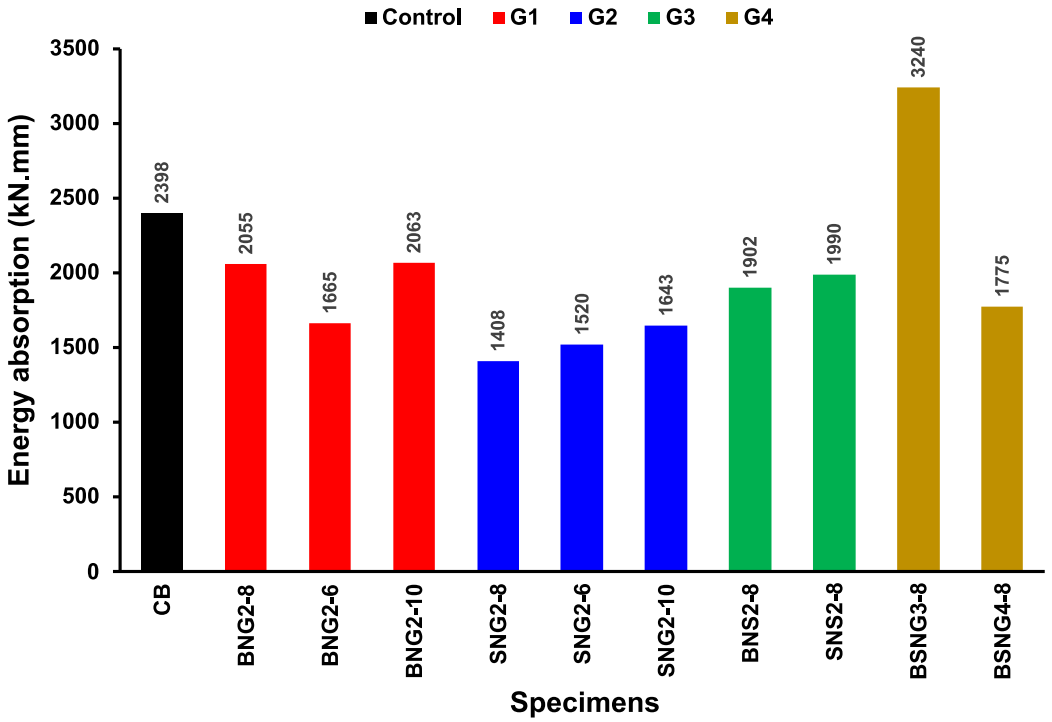

Fig. 7 The energy-absorbing capability of the investigated beams

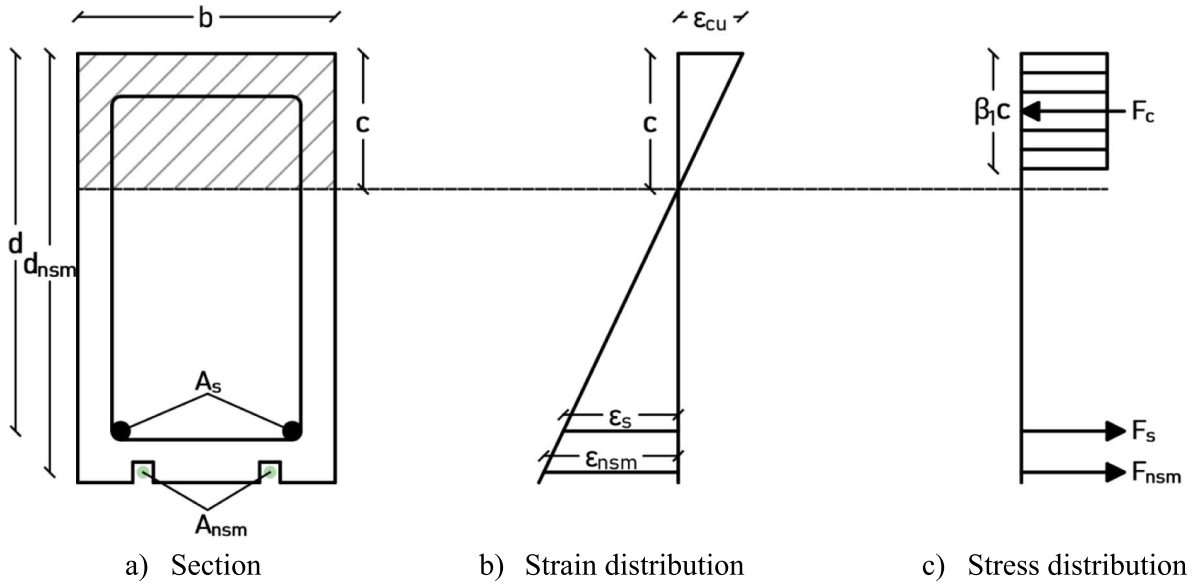

Fig. 8 Strain and equivalent stress distribution for beam section

deflection points (Abdallah et al., 2020). In the current investigation, energy absorption capacity was measured using the area under the load against mid-span deflection curves shown in Fig. 4, up to the ultimate load. Table 5 enumerates the findings and depicts them graphically in Fig. 7.

Except for BSNG3-8, the strengthened beams had lower energy absorption capabilities than compared to the reference beam. SNSM GFRP beams had lower energy absorption capacities than BNSM GFRP beams. In contrast, the SNSM steel specimen has shown

enhanced energy absorption capacities than the BNSM steel specimen. The bottom and side GFRP specimens demonstrated better bending performance than the corresponding steel equivalents. Nevertheless, steel specimens had better energy absorption capabilities. The hybrid distribution of GFRP bars in the BSNG3-8 demonstrated the maximum flexure and energy absorption capacities, outperforming all other evaluated beams in this study. Although the BSNG4-8 had the highest amount of NSM reinforcement, the ineffective distribution of the reinforcement led to premature debonding, preventing the specimen from achieving full flexural strength and leading to low energy absorption capability.

4 Analytical Investigation

4.1 Ultimate Load Prediction

In this work, the ultimate load for NSM strengthened beams is assessed analytically using the ACI 440.2R (2017), based on equilibrium of forces and strain correlation from the analysis of the section illustrated in Fig. 8. The analysis is performed in the constant moment zone assuming failure due to concrete crushing after tension reinforcement yielding.

Equilibrium equation of forces:

$$\mathrm{Fc} = \mathrm{Fs} + \mathrm{Fnsm}, \tag{1}$$

where

Compressive concrete force:

$$\mathrm{Fc} = \mathrm{fc}' \times \mathrm{b}_1 \times \mathrm{b} \times \mathrm{c}, \tag{2}$$

Tensile main reinforcement force:

$$\mathrm{Fs} = \mathrm{As} \times \mathrm{fy}, \tag{3}$$

Tensile NSM bars force:

$$\mathrm{Fnsm} = \mathrm{Ansm} \times \mathrm{fnsm} = \mathrm{Ansm} \times \mathrm{Ensm} \times \mathrm{ensm}. \tag{4}$$

The maximum NSM bars strain, corresponding to the ultimate load, was evaluated using the similarity of triangles assuming the ultimate compressive strain in concrete to be equal to 0.003:

$$\varepsilon\mathrm{nsm} = \varepsilon\mathrm{cu} \times \frac{\mathrm{d_{nsm}} - \mathrm{c}}{\mathrm{c}} \leq \varepsilon\mathrm{nsmu}, \tag{5}$$

where:

$$\varepsilon\mathrm{nsmu} = \frac{\mathrm{f_{nsm_u}}}{\mathrm{E_{nsm}}}. \tag{6}$$

Using the previous formulae, the location of the neutral axis might be computed using the following relation:

$$(\mathrm{fc}' \times \mathrm{b}_1 \times \mathrm{b})\,\mathrm{c}^2 + (\mathrm{Ansm} \times \mathrm{Ensm} \times \mathrm{ecu} - \mathrm{As} \times \mathrm{fy})\,\mathrm{c} - \mathrm{Ansm} \times \mathrm{Ensm} \times \mathrm{ecu} \times \mathrm{dnsm} = 0. \tag{7}$$

The ultimate moment could be computed using the following relation:

$$\mathrm{Mu} = \mathrm{As} \times \mathrm{fy} \times (\mathrm{d} - 0.5 \times \mathrm{b}_1 \times \mathrm{c}) + \mathrm{Ansm} \times \mathrm{Ensm} \times \mathrm{ensm} \times (\mathrm{dnsm} - 0.5 \times \mathrm{b}_1 \times \mathrm{c}). \tag{8}$$

Finally, the ultimate load could be computed using the following relation:

$$\mathrm{Pu} = \frac{4 \times \mathrm{M_u}}{\mathrm{L} - \mathrm{a}}, \tag{9}$$

where

Clear span: $L = 1.6$ m,

Distance between two-point loads: $a = 0.45$ m.

Table 6 Experimental vs analytical ultimate loads

Group	Notation	Pu (experimental) (kN)	Pu (calculated) (kN)	Pu (experimental)/ Pu (calculated) (kN)
Control	CB	78.6	70	0.89
G1	BNG2-8	114.2	108.6	0.95
	BNG2-6	104.6	96.5	0.92
	BNG2-10	139.8	119.8	0.86
G2	SNG2-8	106.3	102.9	0.97
	SNG2-6	93.0	91.9	0.99
	SNG2-10	120.8	113.7	0.94
G3	BNS2-8	105.3	90.3	0.86
	SNS2-8	101.6	88.5	0.87
G4	BSNG3-8	140.9	115.1	0.82
	BSNG4-8	134.6	125	0.93
Average				0.91

4.2 Analytical and Experimental Results Comparison

The results for the ultimate load (Pu), obtained both analytically and experimentally, are summarized in Table 6. The experimental-to-predicted analytical result ratio varies from 0.82 to 0.99%. It can be concluded that the analytical results showed a close prediction of the nominal capacity compared to the experimental investigation.

5 Conclusions

Current research examines the flexure performance of rubberized concrete beams strengthened with bottom, side, and newly proposed hybrid NSM systems. The experimental investigation included 11 RC beams and investigated the influence of several aspects such as strengthening area, distribution, and type. The research

evaluates the load capacities, load–deflection behavior, modes of failure, ductility index, and energy absorption capacities, and the below findings could be identified:

- The NSM technique enhanced rubberized concrete beam flexural performance regardless of strengthening scenario. The load-carrying capacity increased 18–79% over control beam. The initial cracking load enhancement was 17–90%.
- Increasing NSM reinforcement from 57 to 157 mm^2 increased load-carrying capability from 35 to 78% for GFRP BNSM specimens and 18% to 54% for GFRP SNSM specimens. Due to the increased internal arm, BNSM showed a higher loading capacity.
- Steel NSM specimens had lower flexural capacity and stiffness than GFRP specimens, but using steel bars can be cost-effective. The steel BNSM specimen increased its loading capacity by 34%, while the SNSM specimen increased by just 29%.
- The suggested hybrid NSM approach was effective in BSNG3-8, increasing load-carrying capacity by 79%. In contrast, raising the NSM bars to four in BSNG4-8 resulted in excessive stress overlapping and premature debonding, providing only a 71% increase.
- The strengthened beams developed finer, more closely spaced cracks than the reference beam. The GFRP BNSM specimens failed owing to premature debonding. In contrast, the GFRP SNSM and steel specimens showed a more ductile failure and failed due to crushing of concrete after the yielding of main steel. Concrete crushing caused failure in BSNG3-8, whereas in BSNG4-8 it was due to concrete cover separation.
- All strengthened beams had lower mid-span deflection and DI than the reference beam. SNSM is more efficient for DI than BNSM, and steel bars outperform GFRP bars. DI decreased with increasing amount of strengthening reinforcement, except for BSNG3-8, which outperformed all other beams in this study.
- Except for BSNG3-8, all specimens showed a reduction in energy absorption capability.
- Ultimate load capacities were evaluated analytically, and the experimental-to-predicted analytical result ratio varies from 0.84 to 1.01%.
- It is recommended to conduct finite element simulations to validate experimental results and apply models to study additional parameters.
- Additional research is needed to examine the flexural behavior of strengthened beams under sustained and fatigue loading, considering the influence of previous cracking.

Acknowledgements
Not applicable.

Author contributions
Mohamed Emara: investigation, data curation, supervision, writing- original draft preparation, writing—reviewing and editing. Abdulrahman H. Mostafa: resources, investigation, and writing—original draft preparation. Heba A. Mohamed: supervision, reviewing and editing. Mahmoud Zaghlal: investigation.

Funding
Open access funding provided by The Science, Technology & Innovation Funding Authority (STDF) in cooperation with The Egyptian Knowledge Bank (EKB). Not applicable.

Availability of data and materials
Data will be available upon request.

Declarations

Ethics approval and consent to participate
Not applicable.

Consent for publication
All authors have reviewed the manuscript and agreed to its submission for publication.

Competing interests
All authors declare that they have no conflict of interest.

Received: 11 October 2024 Accepted: 13 April 2025
Published online: 17 July 2025

References

Abdalla, J. A., Ali, A. B., Hawileh, R. A., Mhanna, H. H., Galal, K. E., & Saqan, E. I. (2023). Effect of CFRP anchorages on the flexural behavior of externally strengthened reinforced concrete beams. *Archives of Civil and Mechanical Engineering*. https://doi.org/10.1007/s43452-023-00784-7

Abdalla, J. A., Mohammed, A., & Hawileh, R. A. (2020). Flexural strengthening of reinforced concrete beams with externally bonded hybrid systems. *Procedia Structural Integrity*. https://doi.org/10.1016/j.prostr.2020.11.078

Abdallah, M., Al Mahmoud, F., Boissière, R., Khelil, A., & Mercier, J. (2020). Experimental study on strengthening of RC beams with side near surface mounted technique-CFRP bars. *Composite Structures, 234*, 111716. https://doi.org/10.1016/j.compstruct.2019.111716

ACI Committee 440.2R-17. (2017). Guide for the design and construction of externally bonded FRP systems for strengthening concrete structures. ACI Report, American Concrete Institute.

Almusallam, T. H., Elsanadedy, H. M., Al-Salloum, Y. A., & Alsayed, S. H. (2013). Experimental and numerical investigation for the flexural strengthening of RC beams using near-surface mounted steel or GFRP bars. *Construction and Building Materials*. https://doi.org/10.1016/j.conbuildmat.2012.09.107

Al-Saadi, N. T. K., Mohammed, A., Al-Mahaidi, R., & Sanjayan, J. (2019). A state-of-the-art review: Near-surface mounted FRP composites for reinforced concrete structures. *Construction and Building Materials, 209*, 748–769. https://doi.org/10.1016/j.conbuildmat.2019.03.121

Assad, M., Hawileh, R. A., & Abdalla, J. A. (2024). Flexural strengthening of reinforced concrete beams with CFRP laminates and spike anchors. *Composites Part c: Open Access*. https://doi.org/10.1016/j.jcomc.2024.100443

Attari, N., Amziane, S., & Chemrouk, M. (2012). Flexural strengthening of concrete beams using CFRP, GFRP and hybrid FRP sheets. *Construction and Building Materials, 37*, 746–757. https://doi.org/10.1016/j.conbuildmat.2012.07.052

Barros, J. A. O., Dias, S. J. E., & Lima, J. L. T. (2007). Efficacy of CFRP-based techniques for the flexural and shear strengthening of concrete beams. *Cement and Concrete Composites, 29*, 203–217. https://doi.org/10.1016/j.cemconcomp.2006.09.001

Bilotta, A., Ceroni, F., Di Ludovico, M., Nigro, E., Pecce, M., & Manfredi, G. (2011). Bond efficiency of EBR and NSM FRP systems for strengthening concrete members. *Journal of Composites for Construction, 15*, 757–772. https://doi.org/10.1061/(ASCE)CC.1943-5614.0000204

Bilotta, A., Ceroni, F., Nigro, E., & Pecce, M. (2015). Efficiency of CFRP NSM strips and EBR plates for flexural strengthening of RC beams and loading pattern influence. *Composite Structures, 124*, 163–175. https://doi.org/10.1016/j.compstruct.2014.12.046

BS EN 12390-3:2009. (2009). Testing hardened concrete—Part 3: Compressive strength of test specimens.

BS EN 12390-6:2009. (2009). Testing hardened concrete—Part 6: Tensile splitting strength of test specimens.

Ceroni, F., & Pecce, M. (2012). Statistical analysis of debonding load in concrete elements externally strengthened with CFRP materials. *Advances in Structural Engineering, 15*, 155–168.

Darain, K. M. U., Jumaat, M. Z., Hossain, M. A., Hosen, M. A., Obaydullah, M., Huda, M. N., & Hossain, I. (2015). Automated serviceability prediction of NSM strengthened structure using a fuzzy logic expert system. *Expert Systems with Applications*. https://doi.org/10.1016/j.eswa.2014.07.058

De Domenico, D., Fuschi, P., Pardo, S., & Pisano, A. A. (2014). Strengthening of steel-reinforced concrete structural elements by externally bonded FRP sheets and evaluation of their load carrying capacity. *Composite Structures, 118*, 377–384. https://doi.org/10.1016/j.compstruct.2014.07.040

De Lorenzis, L. (2000). Strengthening of RC structures with near surface mounted FRP rods.

De Lorenzis, L., & Teng, J. G. (2007). Near-surface mounted FRP reinforcement: An emerging technique for strengthening structures. *Composites Part b: Engineering, 38*, 119–143. https://doi.org/10.1016/j.compositesb.2006.08.003

Emara, M., Elkomy, N., & Hassan, H. (2021). Numerical assessment of reinforced concrete beams strengthened with CFRP sheets under impact loading. *Frattura Ed Integrita Strutturale-Fracture and Structural Integrity*. https://doi.org/10.3221/IGF-ESIS.58.04

Emara, M., El-Zohairy, A., Fekry, M., & Husain, M. (2022). Effect of using ECC layer on the flexural performance of rc beams previously strengthened with EB CFRP laminates. *Sustainability (Switzerland)*. https://doi.org/10.3390/su142416990

Emara, M., Hamoda, A., & Hu, J. W. (2023a). Numerical assessment of rectangular one- and two-way RC slabs strengthened with CFRP under impact loads. *Computers and Concrete, 31*, 173–184. https://doi.org/10.12989/cac.2023.31.3.173

Emara, M., Salem, M. A., Mohamed, H. A., Shehab, H. A., El-Zohairy, A., & Sharma, A. (2023b). Shear strengthening of reinforced concrete beams using engineered cementitious composites and carbon fiber-reinforced polymer sheets. *Fibers*. https://doi.org/10.3390/fib11110098

Gerges, N. N., Issa, C. A., & Fawaz, S. A. (2018). Rubber concrete: Mechanical and dynamical properties. *Case Studies in Construction Materials, 9*, e00184. https://doi.org/10.1016/j.cscm.2018.e00184

Gopinath, S., Murthy, A. R., & Patrawala, H. (2016). Near surface mounted strengthening of RC beams using basalt fiber reinforced polymer bars. *Construction and Building Materials, 111*, 1–8. https://doi.org/10.1016/j.conbuildmat.2016.02.046

Hawileh, R. A., Nawaz, W., & Abdalla, J. A. (2018). Flexural behavior of reinforced concrete beams externally strengthened with hardwire steel-fiber sheets. *Construction and Building Materials*. https://doi.org/10.1016/j.conbuildmat.2018.03.225

Hawileh, R. A., Nawaz, W., Abdalla, J. A., & Saqan, E. I. (2015). Effect of flexural CFRP sheets on shear resistance of reinforced concrete beams. *Composite Structures*. https://doi.org/10.1016/j.compstruct.2014.12.010

Hawileh, R. A., Rasheed, H. A., Abdalla, J. A., & Al-Tamimi, A. K. (2014). Behavior of reinforced concrete beams strengthened with externally bonded hybrid fiber reinforced polymer systems. *Materials and Design, 53*, 972–982. https://doi.org/10.1016/j.matdes.2013.07.087

Hawileh, R. A., Salama, A. S. D., Mhanna, H. H., Assad, M., Abdalla, J. A., & Saqan, E. I. (2024). Flexural behavior of RC beams externally strengthened with side-bonded CFRP laminates with variable internal reinforcement. *Engineering Structures, 318*, 118707. https://doi.org/10.1016/j.engstruct.2024.118707

Hosen, M. A., Al Kaaf, K. A., Islam, A. B. M. S., Jumaat, M. Z., & Kazmi, Z. A. (2023a). Behavior and modeling of RC beams strengthened with NSM-steel technique. *Structural Engineering and Mechanics*. https://doi.org/10.12989/sem.2023.88.1.067

Hosen, M. A., Jumaat, M. Z., Alengaram, U. J., Islam, A. B. M. S., & bin Hashim, H. (2016b). Near surface mounted composites for flexural strengthening of reinforced concrete beams. *Polymers (Basel)*. https://doi.org/10.3390/polym8030067

Hosen, Md. A., Jumaat, M. Z., Alengaram, U. J., & Ramli Sulong, N. H. (2018). CFRP strips for enhancing flexural performance of RC beams by SNSM strengthening technique. *Construction and Building Materials, 165*, 28–44. https://doi.org/10.1016/j.conbuildmat.2017.12.052

Hosen, M. A., Jumaat, M. Z., Alengaram, U. J., Sulong, N. H. R., & Alsubari, B. (2019). Sustainable palm oil fuel ash mortar used as partial adhesive replacement in flexurally strengthened RC beams. *Construction and Building Materials*. https://doi.org/10.1016/j.conbuildmat.2019.07.222

Hosen, M. A., Jumaat, M. Z., Alsubari, B., Sulong, N. H. R., Ibrahim, Z., Alengaram, U. J., & Hashim, H. (2020). Effect of bonding materials on the flexural improvement in RC beams strengthened with SNSM technique using GFRP bars. *Journal of Building Engineering*. https://doi.org/10.1016/j.jobe.2020.101777

Hosen, M. A., Jumaat, M. Z., & Islam, A. B. M. S. (2015c). Side near surface mounted (SNSM) technique for flexural enhancement of RC beams. *Materials and Design, 83*, 587–597. https://doi.org/10.1016/j.matdes.2015.06.035

Hosen, M. A., Jumaat, M. Z., Islam, A. B. M. S., Kamruzzaman, M., Huda, M. N., & Soeb, M. R. (2015a). Eliminating concrete cover separation of NSM strengthened beams by CFRP end anchorage. *Structural Engineering and Mechanics*. https://doi.org/10.12989/sem.2015.56.6.899

Hosen, M. A., Jumaat, M. Z., Islam, A. B. M. S., Obaydullah, M., Darain, K. M., & Huda, M. N. (2016a). Investigation on energy absorption capacity of reinforced concrete beams by the near-surface mounted technique using ductile materials. *Science of Advanced Materials*. https://doi.org/10.1166/sam.2016.2757

Hosen, M. A., Jumaat, M. Z., & Saiful Islam, A. B. M. (2015b). Inclusion of CFRP-epoxy composite for end anchorage in NSM-epoxy strengthened beams. *Advances in Materials Science and Engineering*. https://doi.org/10.1155/2015/812797

Hosen, M. A., Jumaat, M. Z., Saiful Islam, A. B. M., Al Kaaf, K. A., Shammas, M. I., Hakeem, I. Y., & Ul Islam, M. M. (2023b). Potential side-NSM strengthening approach to enhance the flexural performance of RC beams: Experimental, numerical and analytical investigations. *Structural Engineering and Mechanics*. https://doi.org/10.12989/sem.2023.85.2.179

Hosen, M. A., Jumaat, M. Z., Saiful Islam, A. B. M., Salam, M. A., & Mo, K. H. (2017a). Side-NSM composite technique for flexural strengthening of RC beams. *Computers and Concrete*. https://doi.org/10.12989/cac.2017.20.4.439

Hosen, Md. A., Alengaram, U. J., Jumaat, Z., Sulong, H., & ud Darain, K. M. (2017b). Glass fiber reinforced polymer (GFRP) bars for enhancing the flexural performance of rc beams using side-NSM technique. *Polymers (Basel), 9*, 180. https://doi.org/10.3390/polym9050180

Imjai, T., Setkit, M., Figueiredo, F. P., Garcia, R., Sae-Long, W., & Limkatanyu, S. (2022). Experimental and numerical investigation on low-strength RC beams strengthened with side or bottom near surface mounted FRP rods. *Structure and Infrastructure Engineering*. https://doi.org/10.1080/15732479.2022.2045613

Khalifa, A. M. (2016). Flexural performance of RC beams strengthened with near surface mounted CFRP strips. *Alexandria Engineering Journal, 55*, 1497–1505. https://doi.org/10.1016/j.aej.2016.01.033

Khatib, Z. K., & Bayomy, F. M. (1999). Rubberized Portland cement concrete. *Journal of Materials in Civil Engineering, 11*, 206–213. https://www.tib.eu/de/suchen/id/BLSE%3ARN064516796

Kotynia, R. (2012). Bond between FRP and concrete in reinforced concrete beams strengthened with near surface mounted and externally bonded reinforcement. *Construction and Building Materials, 32*, 41–54. https://doi.org/10.1016/j.conbuildmat.2010.11.104

Kusuma, Y., Rashmi, T., Anand, V. N., & Balaji, N. C. (2022). An experimental study on flexural performance of RC beams strengthened by NSM technique using GFRP strips for a resilient infrastructure system. *Materials Today: Proceedings, 52*, 1959–1967. https://doi.org/10.1016/j.matpr.2021.11.600

Mendis, A. S. M., Al-Deen, S., & Ashraf, M. (2017a). Behaviour of similar strength crumbed rubber concrete (CRC) mixes with different mix proportions.

Construction and Building Materials, 137, 354–366. https://doi.org/10.1016/j.conbuildmat.2017.01.125
Mendis, A. S. M., Al-Deen, S., & Ashraf, M. (2017b). Effect of rubber particles on the flexural behaviour of reinforced crumbed rubber concrete beams. *Construction and Building Materials, 154*, 644–657. https://doi.org/10.1016/j.conbuildmat.2017.07.220
Mhanna, H. H., Hawileh, R. A., & Abdalla, J. A. (2019). Shear strengthening of reinforced concrete beams using CFRP wraps. *Procedia Structural Integrity*. https://doi.org/10.1016/j.prostr.2019.08.029
Mostofinejad, D., & Moghaddas, A. (2014). Bond efficiency of EBR and EBROG methods in different flexural failure mechanisms of FRP strengthened RC beams. *Construction and Building Materials, 54*, 605–614. https://doi.org/10.1016/j.conbuildmat.2014.01.002
Mustafa, S., Shaaban, H., & Elshazly, F. (2020). Rubberized concrete properties and its structural engineering applications—An overview. *Egyptian Journal for Engineering Sciences and Technology, 30*, 1–11. https://doi.org/10.21608/EIJEST.2020.35823.1000
Nawaz, W., Elchalakani, M., Karrech, A., Yehia, S., Yang, B., & Youssf, O. (2022). Flexural behavior of all lightweight reinforced concrete beams externally strengthened with CFRP sheets. *Construction and Building Materials, 327*, 126966. https://doi.org/10.1016/j.conbuildmat.2022.126966
Nayak, A. N., Kumari, A., & Swain, R. B. (2018). Strengthening of RC beams using externally bonded fibre reinforced polymer composites. *Structures, 14*, 137–152. https://doi.org/10.1016/j.istruc.2018.03.004
Rahman, M. M., Jumat, M. Z., Hosen, M. A., & Saiful Islam, A. B. M. (2016). Effect of adhesive replacement with cement mortar on NSM strengthened RC beam. *Revista De La Construccion*. https://doi.org/10.4067/s0718-915x2016000100006
Reda, R. M., Sharaky, I. A., Ghanem, M., Seleem, M. H., & Sallam, H. E. M. (2016). Flexural behavior of RC beams strengthened by NSM GFRP Bars having different end conditions. *Composite Structures, 147*, 131–142. https://doi.org/10.1016/j.compstruct.2016.03.018
Sabau, C., Popescu, C., Sas, G., Schmidt, J. W., Blanksvärd, T., & Täljsten, B. (2018). Strengthening of RC beams using bottom and side NSM reinforcement. *Composites Part b: Engineering, 149*, 82–91. https://doi.org/10.1016/j.compositesb.2018.05.011
Saqan, E. I., Rasheed, H. A., & Hawileh, R. A. (2013). An efficient design procedure for flexural strengthening of RC beams based on ACI 440.2R–08. *Composites Part b: Engineering*. https://doi.org/10.1016/j.compositesb.2013.01.006
Sharaky, I. A., Mohamed, H. A., Torres, L., & Emara, M. (2020). Flexural behavior of rubberized concrete beams strengthened in shear using welded wire mesh. *Composite Structures, 247*, 112485. https://doi.org/10.1016/j.compstruct.2020.112485
Sharaky, I. A., Torres, L., & Sallam, H. E. M. (2015). Experimental and analytical investigation into the flexural performance of RC beams with partially and fully bonded NSM FRP bars/strips. *Composite Structures, 122*, 113–126. https://doi.org/10.1016/j.compstruct.2014.11.057
Shukri, A. A., Hosen, M. A., Muhamad, R., & Jumaat, M. Z. (2016). Behaviour of precracked RC beams strengthened using the side-NSM technique. *Construction and Building Materials*. https://doi.org/10.1016/j.conbuildmat.2016.07.066
Siddika, A., Al Mamun, M. A., Ferdous, W., & Alyousef, R. (2020). Performances, challenges and opportunities in strengthening reinforced concrete structures by using FRPs—A state-of-the-art review. *Engineering Failure Analysis, 111*, 104480. https://doi.org/10.1016/j.engfailanal.2020.104480
Tang, W. C., Balendran, R. V., Nadeem, A., & Leung, H. Y. (2006). Flexural strengthening of reinforced lightweight polystyrene aggregate concrete beams with near-surface mounted GFRP bars. *Building and Environment, 41*, 1381–1393. https://doi.org/10.1016/j.buildenv.2005.05.029
Toutanji, H. A. (1996). The use of rubber tire particles in concrete to replace mineral aggregates. *Cement and Concrete Composites, 18*, 135–139. https://doi.org/10.1016/0958-9465(95)00010-0
Xue, J., & Shinozuka, M. (2013). Rubberized concrete: A green structural material with enhanced energy-dissipation capability. *Construction and Building Materials, 42*, 196–204. https://doi.org/10.1016/j.conbuildmat.2013.01.005
Yasser, N., Abdelrahman, A., Kohail, M., & Moustafa, A. (2023). Experimental investigation of durability properties of rubberized concrete. *Ain Shams Engineering Journal, 14*, 102111. https://doi.org/10.1016/j.asej.2022.102111
Zhang, S. S., Yu, T., & Chen, G. M. (2017). Reinforced concrete beams strengthened in flexure with near-surface mounted (NSM) CFRP strips: Current status and research needs. *Composites Part b: Engineering, 131*, 30–42. https://doi.org/10.1016/j.compositesb.2017.07.072

Publisher's Note

Mohamed Emara is an associate professor at Structural Engineering Department, Faculty of Engineering, Zagazig University, Zagazig in Egypt.

Abdulrahman H. Mostafa is a MSc. student at Structural Engineering Department, Faculty of Engineering, Zagazig University, Zagazig in Egypt.

Heba A. Mohamed is a professor at Structural Engineering Department, Faculty of Engineering, Zagazig University, Zagazig in Egypt.

Mahmoud Zaghlal is an assistant professor at Structural Engineering Department, Faculty of Engineering, Zagazig University, Zagazig in Egypt.